https://doi.org/10.1016/j.colsurfb.2020.111503
This is the Pre-Published Version.

Soft hydrogel promotes dorsal root ganglion by upregulating gene expression of Ntn4 and Unc5B

Guicai Li [1,2*], Shiyu Chen [1,2], Liling Zhang [1,2], Qi Han [1,2], Di Suo[3], Xin Zhao [3*], Yumin Yang [1,2*]

[1]Key laboratory of Neuroregeneration of Jiangsu and Ministry of Education, Nantong University, 226001, Nantong, P.R. China

[2]Co-innovation Center of Neuroregeneration, Nantong University, 226001, Nantong, P.R. China

[3] Department of Biomedical Engineering, the Hong Kong Polytechnic University, Hung Hom, Hong Kong SAR, China

Corresponding author: Guicai Li: gcli1981@ntu.edu.cn; Xin Zhao: xin.zhao@polyu.edu.hk; Yumin Yang: yangym@ntu.edu.cn

Abstract

Mechanical property is an important factor of cellular microenvironment for neural tissue regeneration. In this study, polyacrylamide (PAM) hydrogels with systematically varying elastic modulus were prepared using *in situ* radical polymerization. We found that the hydrogel was biocompatible, and the length of dorsal root ganglion (DRG)'s axon and cell density were optimal on the hydrogels with elastic modulus of 5.13 kPa (among hydrogels with elastic modulus between 3.57 kPa and 16.50 kPa). These DRGs also exhibited highest gene and protein expression of proliferation marker Epha4, Ntn4, Sema3D and differentiation marker Unc5B. Our study revealed the mechanism of how material stiffness affects DRG proliferation and differentiation. It will also provide theoretical basis and evidence for the design and development of nerve graft with better repair performance.

Keywords: Polyacrylamide, stiffness, dorsal root ganglion, gene and protein expression

1. Introduction

Peripheral nerve injury (PNI) is a common clinical disease in the world, which seriously affects the health and life of patients and causes a huge burden to individuals and society [1-4]. According to the statistics of the world health organization, there are about 1 million new cases of nerve injury in China every year, among which about 300,000 cases are peripheral nerve injury (PNI) [5]. PNI has become a common disease, and its repair has been an urgent problem in modern medicine. At present, the traditional autologous nerve is still used as the graft for the treatment of peripheral nerve defects. These autologous nerve transplants, however, have several shortcomings, including limited donor nerves, the need for secondary surgery, lesions in the donor site, and the mismatch between the donor nerve and the recipient site [6, 7]. In recent years, with the development of regenerative medicine, great

© 2020. This manuscript version is made available under the CC-BY-NC-ND 4.0 license https://creativecommons.org/licenses/by-nc-nd/4.0/

progress has been made in the development and application of tissue-engineered nerve grafts to repair nerve defects. For example, hydrogel materials including silk fibroin [8], chitosan [9], hyaluronic acid [10], gelatin [11,12]and sodium alginate[13], have achieved good results in repairing PNI. However, their effect on restoring the sensory function of peripheral nerve is far from ideal as they don't provide appropriate microenvironment for sensory neurons.

As reported, mechanical properties can regulate cell behaviors and functions like cell adhesion, morphology, proliferation and gene and protein expression, thus guiding tissue regeneration and functions[14-17]. However, most of current studies focus on the influence of these materials on neural stem cells while only few studied focused on sensory neuron, dorsal root ganglion (DRGs). DRGs have been widely used in studies on axonal regeneration and guidance, and the generation of myelin sheath of the peripheral nervous system. It is expected that studying the mechanisms on how materials properties affects DRGs and axon growth is crucial to regulate neuron behaviors and functions[17-19]. Unfortunately, detailed influence and mechanism of material stiffness on DRGs for peripheral nerve regeneration, remain unknown.

Therefore, in this study, we fabricated polyacrylamide (PAM) hydrogels of different bis-acrylamide concentration by in-situ radical polymerization. We characterized the morphology, surface and internal structure, swelling ratio and mechanical properties of these PAM hydrogels. We also characterized the cytocompatibility of the hydrogel materials and examined the effect of modulus of PAM hydrogels on growth and differentiation of DRGs in terms of gene and protein expression. We found that the material elasticity had a significant effect on DRG behavior and functions by regulating the gene and protein expression of Epha4, Ntn4, Sema3D and Unc5B. We expect the mechanism we elucidate on how materials stiffness affects DRG behaviors and functions will help design and development of appropriate microenvironment for peripheral neural repair.

2.Materials & Methods

2.1. Materials

Acrylamide, N-N-methylene bis-acrylamide and dopamine were purchased from Sigma Aldrich, USA. Anhydrous sodium carbonate, glycerin and sodium hydroxide were from XiLong Chemical Co. Ltd, China. Anhydrous ethanol and paraformaldehyde were from Zhenxing Chemical Factory, Shanghai, China. Phosphate buffer brine (PBS) was from Hyclone Co. Ltd. Ammonium persulfate, penicillin-streptomycin (PS), MTT cell proliferation and toxicity kit were from Beyotime biotechnology, Shanghai, China. Dulbecco's modified Eagle's medium (DMEM), neurobasal (NB) medium, fetal bovine serum (FBS), B-27 complement and collagenase were from Gibco, USA. 0.25% trypsin-EDTA was from Invitrogen (Carlsbad, CA). L-polylysine and nerve growth factor (NGF)

were from Sigma Aldrich, USA. Bovine serum albumin (BSA) was from Gibco. Anti-neurofilament (NF) antibody, anti-Sema3D antibody, Eph receptor A4 (Epha4) antibody, anti-netrin 4 (Ntn4) antibody and Hoechst 33342 were from Abcam, UK. Primers used in all experiments were made by microporous deionized water purification devices (resistivity > 18.2 M Ω· cm).

2.2. Preparation of PAM hydrogels with various modulus

In this study, we constructed PAM hydrogels with different elastic modulus by changing the content of bis-acrylamide. Mixture containing 29% of acrylamide and 0.06%, 0.18%, 0.36%, 0.5%, 1% or 5% of bis-acrylamide, 10% of ammonium persulfate was prepared. The mixture was added in the petri dish and heated at 55°C. After gelation, the hydrogels were taken out from the petri dish and placed in a foam box filled with water. The samples were then freeze-dried until further use.

2.3. Physical characterization of PAM hydrogels

a. Morphological observation

The surface and cross-sectional morphology of the hydrogels were observed using scanning electron microscopy (SEM, JEOL, Japan). The hydrogel was cut into two parts from the middle with an S35 blade, divided into surface groups and cross-section groups. A gold layer about 50 nm thickness was sprayed on the surface of the sample, and then fixed on an aluminum table. Different multiples were selected for observation under vacuum conditions of 1.4×10^{-4} bar.

b. Porosity

The samples were immersed in anhydrous ethanol of a certain volume (V_1) in the measuring cylinder for 10 min. The total volume of the measuring cylinder after ethanol immersion in the hydrogel was recorded as V_2. The volume of remaining ethanol after taking out the hydrogel was V_3, and three parallel samples were used for each sample. The calculation formula of porosity was: Porosity (%)= $(V_1-V_3) / (V_2-V_3)\times100\%$.

c. Swelling ratio

The initial mass of the freeze-dried hydrogel was measured as W_0, and the initial length, width and height were measured. The volume was recorded as V_0. The freeze-dried hydrogels were put in PBS (pH = 7.2). The interval time was set as 10 min, 20 min, 30 min, 60 min, 90 min, 120 min, 240 min, 720 min, 1 d, 3 d and 5 d. The samples were weighed after the residual liquid on the surface was sucked dry with filter paper, and the mass was recorded as W_1. The length, width and height of hydrogels were recorded, and the volume was calculated as V_1. The swelling rate is calculated

according to: SRm= $(W_1-W_0)/W_0 \times 100\%$; SRv= $(V_1-V_0)/V_0 \times 100\%$

d. Mechanical property

The mechanical properties of PAM hydrogels were tested using electronic universal testing machine (TFW-58, Shanghai Extension Equipment Technology Co., Ltd.). The diameter and height of the hydrogel samples were measured before the test. The universal testing machine was set in the compression model with the speed of 10 mm/min. The elastic modulus was calculated as the slope of stress-strain curve.

2.4. Biological characterization of PAM hydrogels

a. Cytocompatibility

L929 fibroblasts with a density of 5×10^4 cells/mL were seeded on top of hydrogel samples with 10 mm diameter for 24 h. Cell viability was measured using MTT assay according to manufacturer's protocol.

b. Culture of dorsal root ganglion

DRGs were obtained from 1d Sprague-Dawley rats and the connective tissue were stripped. Collagenase was added to DRGs and digested at 37℃ for 30 min. Afterwards, trypsin was added to further digest the tissue at 37℃ for 10 min, and DMEM complete medium was added to terminate the digestion. After centrifugation, the DRGs were cultured at a cell density of 1×10^5 cell/mL. After 4-6 hours of culture, the DMEM complete medium was changed to the NB medium for DRG culture.

c. Immunofluorescence staining

The DRGs were fixed with 4% paraformaldehyde solution for 4 h and then washed with PBS for 2 times, each time for 5 min. Afterwards, the sealing solution was added to each sample and sealed at 37°C. The sealing solution was discarded after 1 h. The hydrogels were treated with primary antibody [NF(1:400)] at 4°C overnight. Then the hydrogels were washed with PBS for 2 times, each time for 5 min. After that, the hydrogels were treated with the secondary antibody [Alexa-488(1:400)] for 2 h at 37°C in dark. The hydrogels were then treated with Hoechst 33342 for 5 min. Finally, the samples were washed with PBS for 3 times and observed by a fluorescence microscope (Leica, Germany).

d. Transcriptome sequencing

The DRGs cultured for 3 days on hydrogels were collected with Trizol reagent (Invitrogen, Carlsbad, CA), and kept in dry ice. The samples were sent to the company (GENEWIZ Biological Technology

Co., Ltd, Suzhou, China) for transcriptome sequencing analysis. According to the results of transcriptome sequencing, differential genes and related pathways were screened out for analysis.

e. Real-time quantitative polymerase chain reaction

RNA was extracted from the DRGs using the Trizol reagent. Then the cDNA was obtained from RNA using the Takara kit (Invitrogen, Carlsbad, CA). The sequence of the primers required in this experiment is listed in Table 1.

Table1. Primer sequences used in Real-time quantitative polymerase chain reaction

Targets	Sequences（5'- 3'）
GAPDH-sense	AACGACCCCTTCATTGAC
GAPDH-antisense	TCCACGACATACTCAGCAC
Ntn4-sense	CTGCAACCCTCGAATGGGAA
Ntn4-antisense	AGTGTCCGCCTGGAGTTTTC
Sema3d-sense	TCCGTGTGCTTCAACCCTAC
Sema3d-antisense	GCTCCAGTTCCACACACGTA
EpHa4-sense	GTCTGAGCCAGTACCGAACA
EpHa4-antisense	ATTTCAGAGGGCGAAGACGA
Unc5B-sense	GGGACGCTACTTGACTCCAA
Unc5B-antisense	AGTTCTCTGATTCAGCACGC

f. Western blot

DRGs were washed with PBS for twice and then were treated with cell lysis solution. After centrifugation at 12,000 rpm for 15 min, the supernatant was taken and the total protein concentration was measured by protein assay kit (Bio-Rad). The proteins were isolated using SDS-PAGE and transferred to polyvinylidene fluoride (PVDF) membrane. The membrane was sealed with 5% skim milk for 90 min and then incubated with primary antibody at 4℃ overnight. The PVDF membrane was washed with tris buffered saline tween (TBST) three times, each time for 10 min. After that, the PVDF membrane was intubated with secondary antibodies for 1 h at 37℃. The PVDF membrane was then washed with TBST for 3 times, each time for 10 min. The electrochemiluminescence (ECL) highly sensitive luminescent solution was added for luminescence imaging.

2.5. Statistical analysis

All the data in this paper were analyzed using Image J and Origin 9.0 (Origin Lab company). The

results were expressed as mean ± standard deviation (n = 3). The results were considered as significant (*p< 0.05, **p < 0.01, ***p < 0.001).

3. Results and discussion

3.1. Physical properties of PAM hydrogels

3.1.1. Elastic modulus of PAM hydrogels with different bis-acrylamide concentration

Fig.1Ai and ii show the stress-strain curves and the elastic modulus of the PAM hydrogels. We found that the elastic modulus increased continuously from 3.57 kPa to 16.50 kPa with the increasing concentration of bis-acrylamide (from 0.06% to 5%).

3.1.2. Morphology of PAM hydrogels with different modulus

The hydrogels with different modulus were observed using SEM. Fig.1Bi and S1 show that the pores on the surface or inside the hydrogels became smaller with increasing modulus. Also, the number of pores inside or on the surface of the hydrogels increase with decreasing elastic modulus.

3.1.3. Pore density and porosity

All hydrogels showed a certain porosity, which was conducive to cell metabolism and supply of nutrients (Fig. 1C). Fig.1Ci) shows that the surface pore density of hydrogel was 348.4 number/mm^2 when the modulus of the hydrogel was 3.57 kPa. With the increasing modulus of hydrogels, the surface pore density of hydrogel was 16 number /mm^2 when the modulus of the hydrogel was 16.50 kPa. Fig.1Cii shows the internal pore density of the hydrogel was 304 number /mm^2 when the elastic modulus of hydrogel was 3.57 kPa. With the increasing modulus of the hydrogels, the internal pore density of the hydrogel was 32 number/mm^2 when the elastic modulus of hydrogel was 16.50 kPa. Fig.1Ciii shows that the porosity was 77 % when the elastic modulus of hydrogel was 3.57kPa. With the increase of the modulus of hydrogels, the porosity decreased to 55%.

3.1.4. Swelling ratio

The swelling ratio of PAM hydrogels with different elastic modulus by volume and mass are shown in Fig.1(Di) and (Dii), respectively. PAM hydrogels gradually reached equilibrium swelling with time. The swelling ratio was the highest with the lowest elastic modulus. The swelling ratio of volume could reach 756 % and the swelling ratio of mass could reach 1304 % when the elastic modulus of hydrogel was 3.57 kPa. The swelling ratio of volume reached 89 % and swelling ratio of mass reached 283% when the elastic modulus of hydrogel was 16.50 kPa. The above results have demonstrated that the hydrogels with the lowest elastic modulus had the highest swelling ration in terms of mass and

volume due to the highest porosity, which is consistent with the results of porosity and SEM.

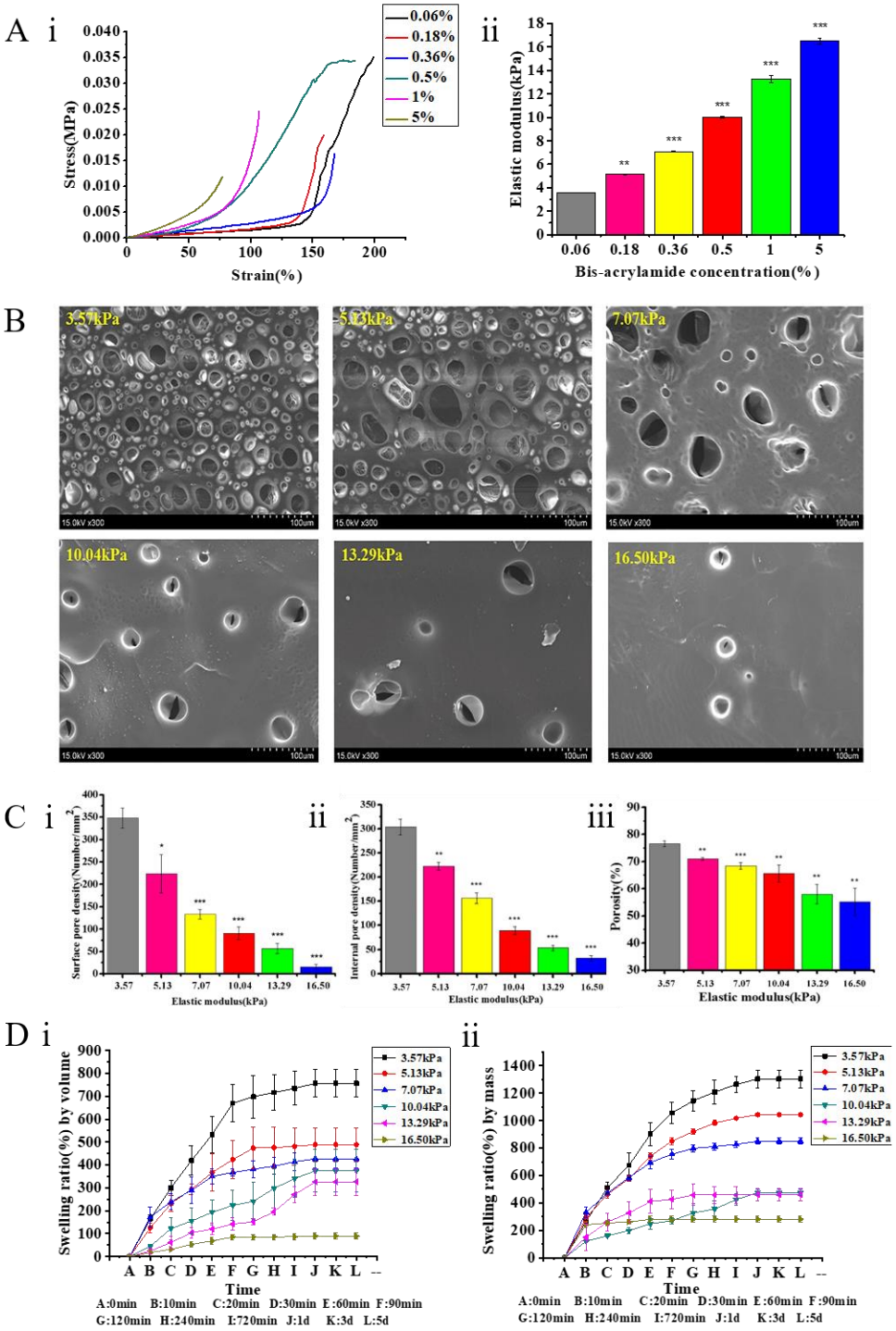

Figure 1. Physical characteristics of PAM hydrogel. (A) Mechanical analysis of PAM hydrogels. (Ai) Stress-strain curve and (Aii) elastic modulus. (B) Surface topography of hydrogels with different modulus. (C) Pore distribution and porosity of hydrogels with different modulus. (Ci) Surface pore density; (Cii) internal pore density; (Ciii) porosity. (D) Swelling rate of hydrogels with different modulus: (Di) swelling ratio by volume and (Dii) swelling ratio by mass. * $p < 0.05$, ** $p < 0.01$ and *** $p < 0.001$

3.2. Biological properties of PAM hydrogels

3.2.1. Effect of modulus of PAM hydrogels on cytocompatibility and cell adhesion

a. Cytocompatibility

Fig.S2 shows the cytocompatibility evaluation of hydrogels. The average OD_{570} absorbance (indicating the number of living cells) of the hydrogels with different stiffness was 0.581, 0.641, 0.668, 0.575, 0.626 and 0.572, which are comparable with the absorbance of the control group (0.533), indicating the cytocompatibility of the PAM hydrogels.

b. Cell adhesion

Fig.2A shows the morphology of DRG on the hydrogel with different stiffness. As shown in Fig.2B and C, the length of axon reaches 347± 26 μm and the cell density reaches 29±4 number/mm^2 when the elastic modulus was 5.13kPa.

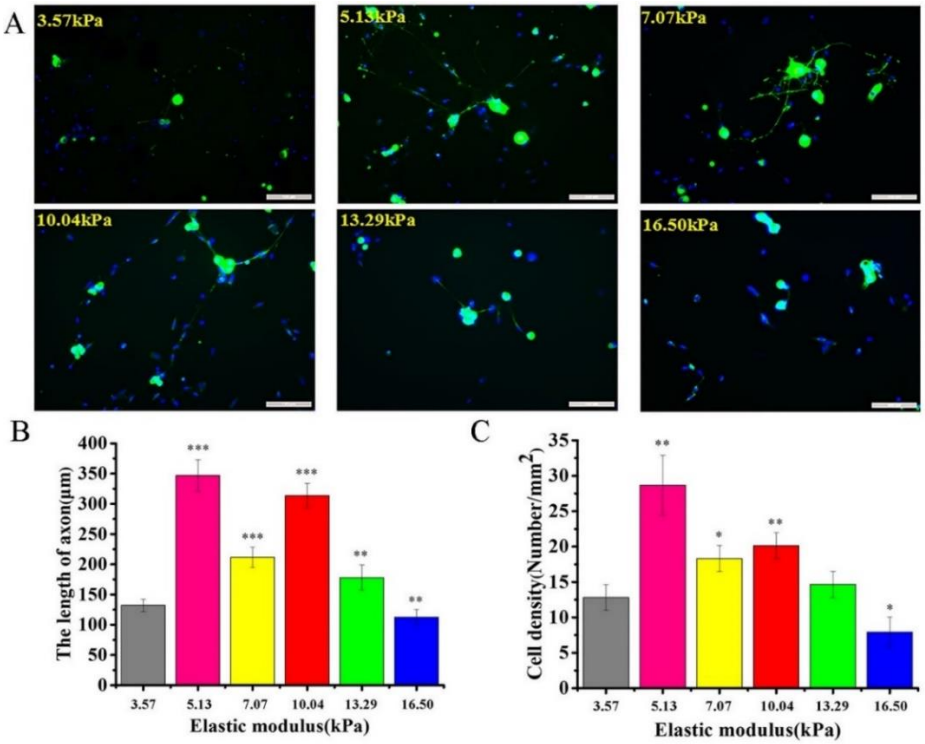

Figure 2. Effect of modulus of PAM hydrogels on cell adhesion. (A) Morphology of DRG (green: neurofilament, NF; blue: nucleus; scale: 100 μm). (B) and (C) Quantification of length of axon and cell density, respectively, *$p < 0.05$, **$p < 0.01$, and *** $p < 0.001$.

3.2.2. Effect of modulus of PAM hydrogels on cell differentiation

a. Gene expression

i) KEGG analysis of differential genes

Different genes perform different biological functions and coordinate with each other. According to

the significant enrichment analysis of pathway, the most important biochemical metabolic and signal transduction pathways involved in the differential genes could be identified [20]. In this study, we used KEGG (Kyoto Encyclopedia of Genes and Genomes) database to identify the differentiation pathway. Fig.S3A shows bar chart of significantly enriched KEGG annotation classification. It was found that there was a pathway of axon guidance. Fig.S3B shows the scatter plot of KEGG enrichment of differential genes. The horizontal axis represented the Rich factor. The size of the dots indicated the number of differential genes in this pathway. The vertical axis represented the name of the pathway. The greater the Rich factor was, the greater the degree of enrichment was. These results demonstrated that lysine biosynthesis, indole alkaloid biosynthesis and C5-branched dibasic acid metabolism were significantly enhanced.

ii) GO analysis of differential genes

We used Gene Ontology (GO), an internationally standardized gene function classification system, to elucidate the information involved in molecular function, biological process, and cellular component. Fig. S4 shows differential genes were mainly involved in positive regulation of transcription from RNA polymerase II promotors, multicellular development, immune response, axon guidance and homopHilic cell adhesion, etc. The main functions of differential genes were in the perinuclear region of cytoplasm, neuronal cell body, cell junction, cell surface, axon, etc, in the part of cell components. In the part of molecular function, the functions involved in differential genes were protein domain specific binding, growth factor activity, heparin binding, protein c-terminus binding, calmodulin binding, etc.

iii) Volcano plot of differential genes

Fig. 3Ai-v shows volcano plot of differential genes between groups (number represented the stiffness of hydrogels), reflecting the distribution of differential genes between two samples. The abscissa represented the fold change of gene expression in different samples. The genes with larger differences were distributed at both ends. The ordinate represented the statistical significance of the difference in gene expression changes. The larger the fold difference, the more significant the statistical difference of genes. The red dots of the differential genes indicated up-regulation and the blue dots indicated down-regulation. It could be seen that all groups had the up-regulated and down-regulated differential genes. From the Volcano plot, the genes corresponding to the pathway with axon guidance and differential genes were screened out. To facilitate the verification, according to the comparison of up-regulated and down-regulated genes, three types of up-regulated differential genes were finally selected: Epha4, Ntn4, and Sema3D. These genes are involved in the development of the nervous

system and in the regulation of axon guidance. As reported, Sema3D plays an important role in the growth of neurons [21]; Ntn4 provided active regulation of axonal migration [22]; and Epha4 played an important role in spinal motor neurons, and its expression could trigger the positive signal transmission of axon movement [23].

iv) Expression of differential genes on hydrogels with different stiffness

Fig.3Bi-iii shows the expression of differential genes of DRG on hydrogels with different stiffness. It could be observed that the relative expression levels of three differential genes were the highest when the elastic modulus was 5.13kPa. The relative expression levels of the other five groups are relatively low. This trend was also consistent with the statistical results of immunofluorescence staining.

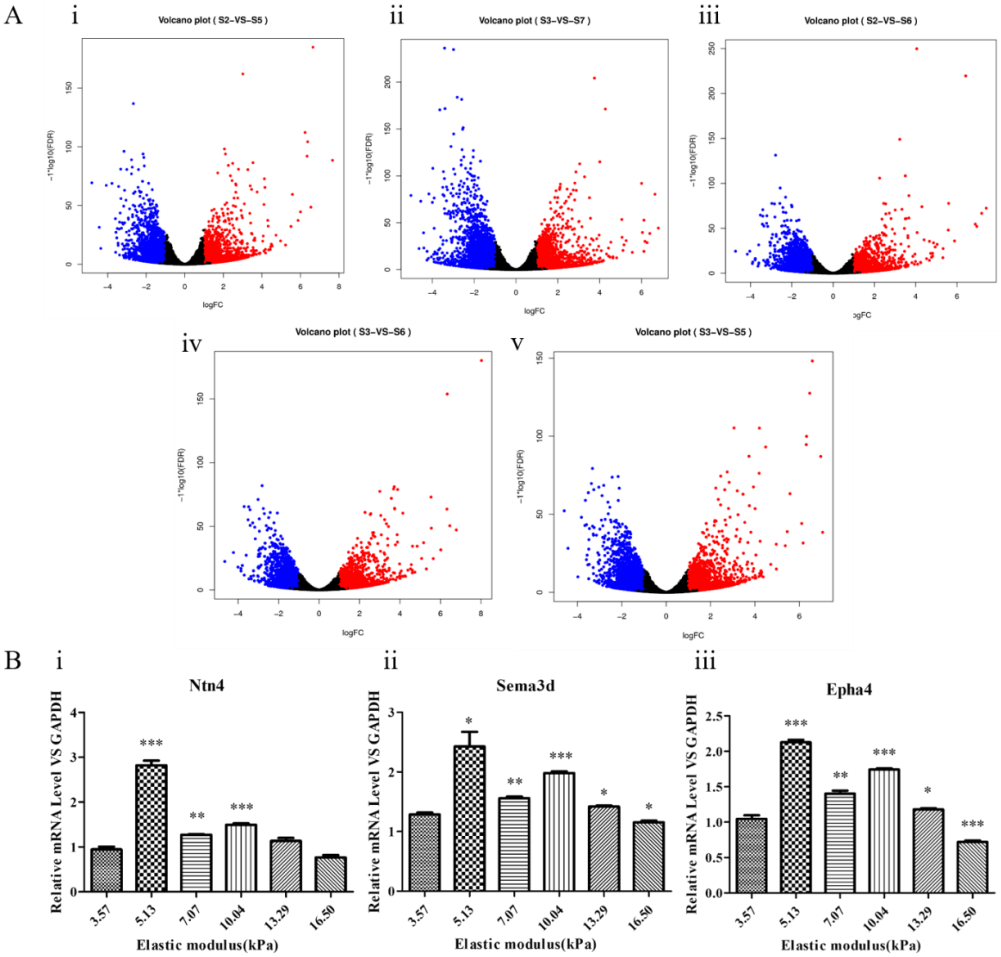

Figure 3. Effect of modulus of PAM hydrogels on cell differentiation. (A) Volcano plot of differential genes between hydrogels with different stiffness (i-v). (B) Relative expression levels of differential genes on hydrogels with different stiffness (i) Ntn4, (ii) Sema3d and (iii) Epha4, *p < 0.05, **p < 0.01 and *** p < 0.001.

b. Protein expression

Fig.4 shows the expression of related proteins on PAM hydrogels with different elastic modulus. Fig.4A shows the band of western blot. Fig.4B-E were the quantification of protein expressions of Ntn4, Sema3D, Epha4 and Unc5B, respectively. The expression level of Ntn4, Epha4 and Sema3d was higher than that of the other five groups when the modulus of hydrogel was 5.13kPa. Moreover, the 5.13 kPa hydrogel group exhibited also enhanced Unc5B expression. Unc5B has been reported to be a mediator of Ntn4 promoting the growth of neurons [22]. The above results have suggested the hydrogel with a modulus of 5.13 kPa could significantly increase the expression level of Ntn4, Sema3D, Epha4 and Unc5B, and promote the growth of DRG.

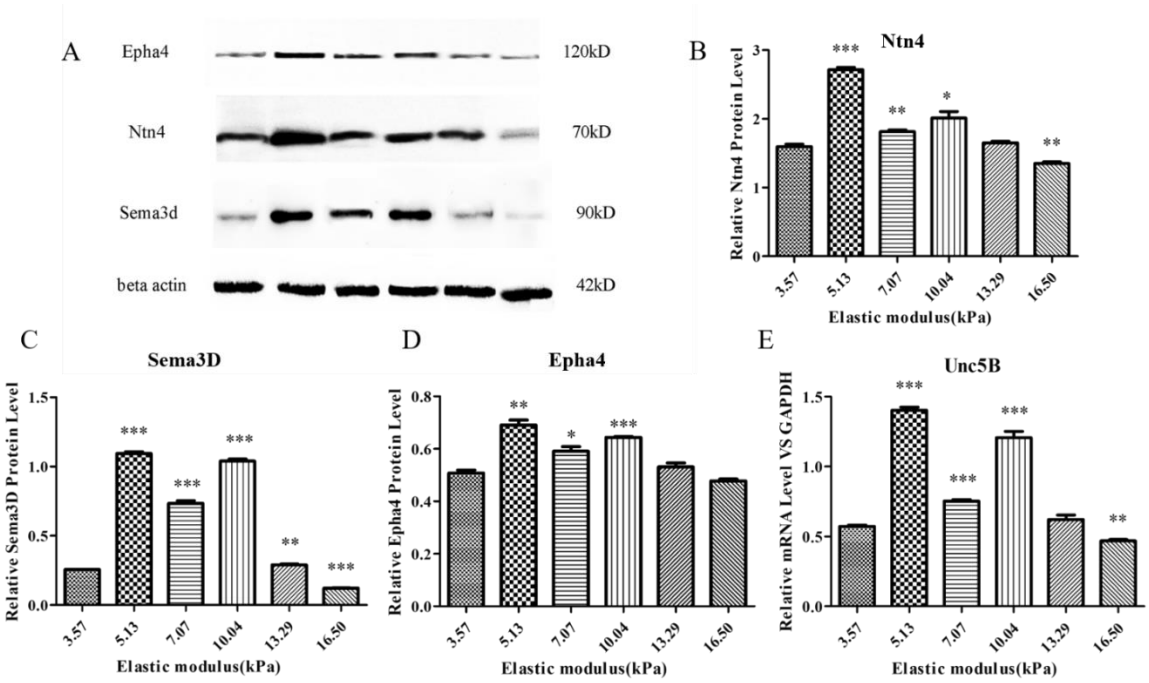

Figure 4. Western blot (A) and quantification of relative expression levels of proteins on hydrogels including (B) Ntn4, (C) Sema3D, (D) Epha4 and (E) Unc5B, *$p < 0.05$, **$p < 0.01$ and *** $p < 0.001$.

3.2.3. Pathway analysis

The stiffness of PAM hydrogel affected the proliferation of DRG. From the above results, we speculated that Sema3D affected the interaction between axons of DRG on hydrogel. The high expression of Sema3D positively regulated the interaction between axons and promoted the growth of DRG. Epha4 could trigger the forward signal conduction of DRG axon movement. Then the Ntn4 provides positive effects on DRG axon migration. As reported, Unc5B was a mediator of Ntn4 in promoting the growth of neurons, and the growth of neurons is inhibited when the expression of Unc5B was low [22]. At optimal stiffness (5.13 kPa), the expression of Ntn4 was raised, leading to upregulated expression of Unc5B and enhanced growth of DRG. Furthermore, in the nervous system,

axons are attracted and repelled. RGMa, a homologue of the rejection guidance molecule (RGM), plays a repulsive guidance role, and RGMa can activate RhoA in neurons[24, 25], and the activation of RhoA has been shown to inhibit the growth of neurons[26]. We hypothesize the increased expression of Unc5B inhibited the activation and axonal rejection of RhOA by RGMa[27] and thus promoted the growth of neurons.

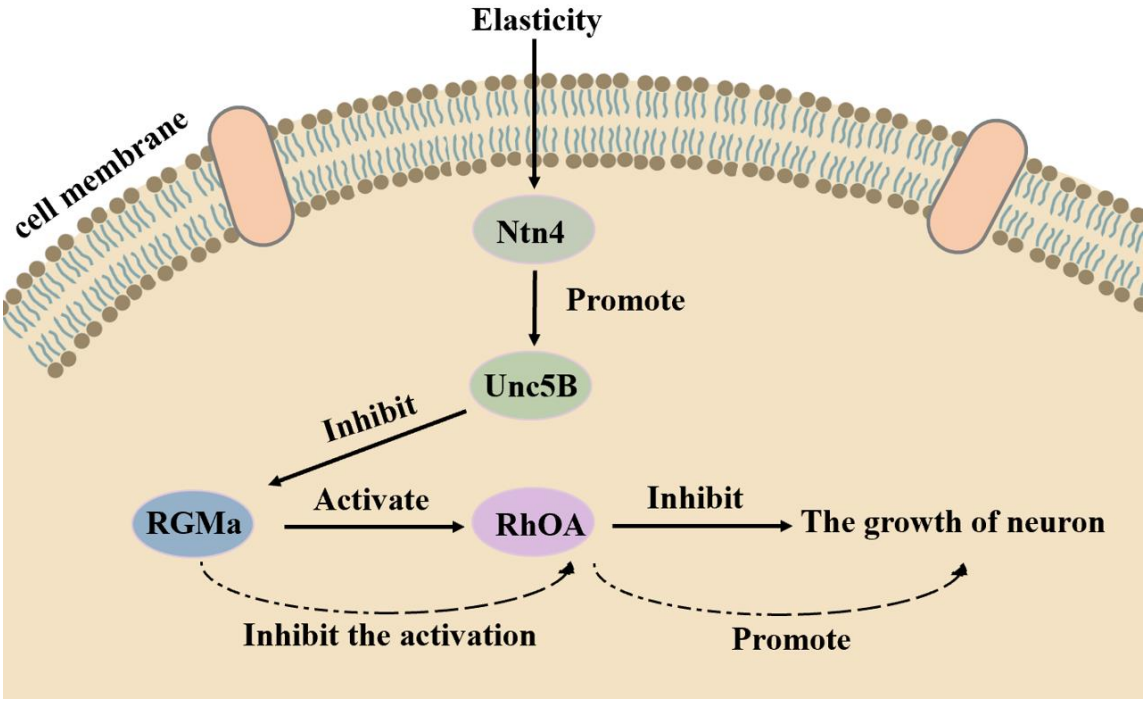

Figure 5. Proposed signal pathway on how stiffness of PAM hydrogel affects proliferation of DRG.

4. Conclusion

In conclusion, this study explored the influence of PAM hydrogels with different modulus on the behavior and function of DRG and revealed the underlying mechanism. According to a series of results, the axon growth and cell density of DRG were optimal when the modulus of hydrogel was 5.13 kPa. The stiffness of the hydrogel was proved to control the growth of DRG's axons by regulating the expression of Ntn4, Sema3D and Epha4 in cells. The upregulated expression of Ntn4 further promoted the expression of Unc5B, and thus the growth of DRG. We believe that the present study based on modulus-cell-gene-signal pathway reveals the relationship between materials stiffness and cell behavior for nerve regeneration, which offers a solid theoretical basis for the design and preparation of nerve grafts to repair peripheral nerve defects.

Acknowledgement

The authors gratefully acknowledge the financial support of the National Natural Science Foundation of China (31830028, 31771054, 11702233), Natural Key Science Research Program of Jiangsu

Education Department (19KJA320006), National Key Research and Development Program of China (2016YFC1101600), 226 High-level Talent Training Project (2nd level, 2018 II-182) of Nantong City, Qinglan Project of Jiangsu Province (2018).

References

1. J. Noble, C. A. Munro, V. S. Prasad and R. Midha, *J Trauma.*, 1998, **45**, 116-122.
2. L. R. Robinson, *Muscle nerve.*, 2000, **23**, 863-873.
3. C. A. Taylor, D. Braza, J. B. Rice and T. Dillingham, *Am J Phys Med Rehabil.*, 2008, **87**, 381-385.
4. M. Asplund, M. Nilsson, A. Jacobsson and H. von Holst, *Neuroepidemiology*, 2009, **32**, 217-228.
5. Y. Gu, J. Zhu, C. Xue, Z. Li, F. Ding, Y. Yang and X. Gu, *Biomaterial.*, 2014, **35**, 2253-2263.
6. M. E. Ortiguela, M. B. Wood and D. R. Cahill, *J Hand Surg Am.*, 1987, **12**, 1119-1123.
7. S. E. Mackinnon and A. R. Hudson, *Plast Reconstr Surg.*, 1992, **90**, 695-699.
8. L. P. Yan, J. M. Oliveira, A. L. Oliveira, S. G. Caridade, J. F. Mano and R. L. Reis, *Acta Biomater.*, 2012, **8**, 289-301.
9. P. Yu, H.-Q. Wang, R.-Y. Bao, Z. Liu, W. Yang, B.-H. Xie and M.-B. Yang, *ACS Sustain Chem Eng.*, 2017, **5**, 1557-1566.
10. S. Han, D. H. Kim, J. Sung, H. Yang, J. W. Park and I. Youn, *Biochem Biophys Res Commun.*, 2019, **508**, 348-353.
11. L. Han, J. Xu, X. Lu, D. Gan, Z. Wang, K. Wang, H. Zhang, H. Yuan and J. Weng, *J Mater Chem B*, 2017, **5**, 731-741.
12. Y. Hu, Y. Hong. , N. Y. Shi. , G. Y. Huang.and X. Zhao, *China Sciencepaper*, 2017, **12**, 2770-2776.
13. J. Wang, X. Ying, J. Liu, X. Li and W. Zhang, *Int J Biol Macromol.*, 2015, **81**, 11-16.
14. D. Hoffman-Kim, J. A. Mitchel and R. V. Bellamkonda, *Annu Rev Biomed Eng.*, 2010, **12**, 203-231.
15. L. Yildirimer, Q. Zhang, S. Kuang, C. J. Cheung, K. A. Chu, Y. He, M. Yang and X. Zhao, *Biofabrication*, 2019, **11**, 032003.
16. S. Blaschke, S. U. Vay, N. Pallast, M. Rabenstein, J. A. Abraham, C. Linnartz, M. Hoffmann, N. Hersch, R. Merkel, B. Hoffmann, G. R. Fink and M. A. Rueger, *J Tissue Eng Regen Med.*,

2019, **13**, 960-972.

17. D. Koch, W. J. Rosoff, J. Jiang, H. M. Geller and J. S. Urbach, *Biophys J.* 2012, **102**, 452-460.
18. J. K. Chilton, *Dev Biol.*, 2006, **292**, 13-24.
19. G. Rosso, P. Young and V. Shahin, *Cell Physiol Biochem.*, 2017, **44**, 1263-1270.
20. M. Kanehisa, M. Araki, S. Goto, M. Hattori, M. Hirakawa, M. Itoh, T. Katayama, S. Kawashima, S. Okuda, T. Tokimatsu and Y. Yamanishi, *Nucleic Acids Res.*, 2008, **36**, D480-484.
21. M. A. Wolman, A. M. Regnery, T. Becker, C. G. Becker and M. C. Halloran, *J Neurosci.*, 2007, **27**, 9653-9663.
22. Y. Hayano, K. Sasaki, N. Ohmura, M. Takemoto, Y. Maeda, T. Yamashita, Y. Hata, K. Kitada and N. Yamamoto, *Proc Natl Acad Sci USA.*, 2014, **111**, 15226-15231.
23. G. Gatto, D. Morales, A. Kania and R. Klein, *Curr Biol.* 2014, **24**, 2355-2365.
24. K. Hata, M. Fujitani, Y. Yasuda, H. Doya, T. Saito, S. Yamagishi, B. K. Mueller and T. Yamashita, *J Cell Biol.*, 2006, **173**, 47-58.
25. S. Conrad, H. Genth, F. Hofmann, I. Just and T. Skutella, *J Biol Chem.*, 2007, **282**, 16423-16433.
26. Z. Li, L. Van Aelst and H. T. Cline, *Nat. Neurosci.*, 2000, **3**, 217-225.
27. K. Hata, K. Kaibuchi, S. Inagaki and T. Yamashita, *J Cell Biol.*, 2009, **184**, 737-750.